MAGNETIC RESONANCE METHODS FOR THE CHARACTERIZATION OF THE PORE SPACE IN VUGGY CARBONATES

Girija S. Padhy, Claude Lemaire and Marios A. Ioannidis
University of Waterloo, Waterloo, Canada.

This paper was prepared for presentation at the International Symposium of the Society of Core Analysts held in Trondheim, Norway 12-16 September, 2006

ABSTRACT

Understanding the petrophysical properties of vuggy carbonate rocks is rendered particularly challenging by the extreme complexity of their pore space. Significant variability of carbonate depositional environments and susceptibility of carbonate sedimends to diagenesis results in pore spaces comprising length scales ranging from nanometers to millimetres (and beyond). Characterizing the size distribution and connectivity of pores spanning several orders of magnitude of the length scale is a key issue in carbonate petrophysics that has not been completely resolved. Nuclear spin diffusion in the susceptibility-contrast induced internal field (DDIF-NMR) has been recently proposed for probing multiple length scales in sedimentary rocks. This method has hitherto been applied to only a few samples and its ability to discern the entire spectrum of pore length scales actually present has not been fully evaluated. Motivated by the need to measure the pore size distribution in vuggy carbonate rocks exhibiting structure over disparate length scales, ranging from less than a micron (matrix pores) to millimetres (vugs), we carry out a DDIF-NMR study of real and synthetic vuggy porous media. Synthetic media having controlled amounts of matrix and vuggy porosity serve as standards. They are made by first sintering known amounts of glass beads and calcium carbonate particles of known sizes, and then dissolving the carbonate particles in an acid. DDIF-NMR results are presented for three synthetic and three real vuggy samples. These results are complemented by 3D-MRI data obtained at a resolution sufficient to resolve millimetre-size vugs and independently determine their amount and connectivity. Additionally, mercury porosimetry and statistical image analysis (SIA) of large (3-cm wide), high-resolution images of thin sections are employed to independently determine the complete pore size distribution. Several assumptions behind the interpretation of DDIF-NMR data (fast diffusion, weak encoding and weak pore coupling conditions uniformly fulfilled for pores of all sizes) and the obvious upper and lower detection limits of this technique are likely reasons for the fact that pore size distributions determined by DDIF-NMR and SIA exhibit only qualitative agreement. Nevertheless, DDIF-NMR provides quantitative information about the fraction of total porosity due to presence of vugs which agrees with the independent results obtained from 3D-MRI. A deeper analysis of the precise origin of the deviations between DDIF-NMR and SIA results must await the development of a more rigorous method for the interpretation of DDIF-NMR data.

BACKGROUND

The capillary pressure, relative permeability and electrical resistivity characteristics of vuggy carbonate rocks cannot be understood, let alone predicted, without quantitative information on the relative amounts, size distribution and connectivity of matrix and vuggy porosity [1,2]. To this end, both direct (*i.e.*, 2D and 3D imaging) and indirect (*e.g.*, mercury porosimetry, magnetic resonance relaxometry) probes of the microstructure are available, each subject to different resolution limitations or model assumptions.

In particular, the DDIF-NMR method [3, 4] seeks to exploit strong, micro-scale gradients of an internal magnetic field, induced by susceptibility differences between the solid and the pore-filling fluid, to determine the pore size distribution. A radio-frequency (RF) pulse sequence $\pi/2-t_e-\pi/2-t_d-\pi/2-t_e-echo$ works by first encoding space-dependent phase differences of spin magnetization as a spatial pattern of amplitudes during an encoding time t_e. Subsequently, the spins undergo molecular self-diffusion and spin-lattice relaxation over time t_d, their position is decoded with the identical internal field over time t_e and an echo signal is acquired. This is repeated for a sequence of diffusion times t_d. A reference pulse sequence serves to detect decay of nuclear magnetization due to spin-lattice relaxation alone, information useful in isolating the effect of diffusion in the internal field. This reference pulse sequence is implemented by $\pi/2-t_e-\pi-t_e-\pi/2-t_d-\pi/2-FID$. Interpretation of DDIF-NMR data is based on the general solution of the Torrey-Bloch equation governing the evolution of spin magnetization:

$$m(r,t)=e^{-\mu t}\sum_{n=0}^{\infty}a_n\phi_n(r)e^{-t/\tau_n}\ , \tag{1}$$

where $m(r,t)$ stands for the fraction of initial magnetization, τ_n and $\phi_n(r)$ are the eigenvalues and eigenfunctions, respectively, and $\mu=1/T_{1b}$ is the bulk spin-lattice relaxation rate. The eigenfuntions are normalized over the pore volume and in the fast-diffusion regime, *i.e.* when $\rho d/D<<1$ where ρ is the surface relaxivity and *D* is the bulk diffusion coefficient, the measured echo is given by [3]:

$$E(t_d)=a_0e^{-t_d/\tau_0}e^{-\mu t_d}+\sum_{n=1}^{\infty}a_ne^{-t_d/\tau_n}e^{-\mu t_d}\ . \tag{2}$$

The first part on the right hand side of Eq. (2) represents the contribution of the lowest mode (ground state) to the measured echo. In the fast-diffusion regime $\tau_0=\rho\langle S/V\rangle$ is approximately valid, where $\langle S/V\rangle$ is the pore surface-to-volume ratio. The second part on the right-hand side of Eq. (2) represents decay due to diffusion in the internal field. For sufficiently short t_e (weak-encoding), the first diffusion eigenmode (n = 1) is

expected to be predominantly excited so that a one-to-one correspondence between relaxation time τ_n and pore diameter is approximately established:

$$\tau_n = \frac{d^2}{D\pi^2}. \quad (3)$$

To our knowledge, vuggy carbonates have not been previously investigated by DDIF-NMR. A challenge for the interpretation of DDIF-NMR in vuggy carbonates concerns the contribution of the ground state, as it is not generally possible to determine the intensity of the lowest mode, a_0, by comparison of the DDIF and reference signals. Also, when DDIF is monitored over long times t_d (as it is necessary for the study of vuggy porosity), multi-exponential fitting of the measured echo yields the distribution of *apparent* relaxation times, τ_n^{eff}, where $1/\tau_n^{eff} = 1/\tau_n + 1/T_{1b}$, making necessary a correction for bulk relaxation (T_{1b} = 3s for water) prior to application of Eq. (3). Clearly, bulk relaxation sets an upper limit for measurable DDIF relaxation times τ_n and $d \to \infty$ as $\tau_n^{eff} \to T_{1b}$. The smallest detectable pore size is limited by the width of the 90°-pulse, which for the typical 10-μs 90°-pulse is of the order of one micron.

An alternative method of determining the pore size distribution over several decades of the length scale (hereafter referred to as statistical image analysis or SIA) is based on the statistical fusion of small-angle neutron scattering (SANS) and backscatter SEM (BSEM) data and their subsequent interpretation in terms of a polydispersed spherical pore (PDSP) model [5]. An extension of this method has also been developed [6], according to which information obtained from SANS is substituted by a fractal scaling law using a surface fractal dimension obtained from analysis of MIP data. Central to the method is the description of a porous medium in terms of a binary phase function $Z(\mathbf{x})$, taking the value of unity if **x** points to solid and zero otherwise. The microstructure is described in terms of the first two moments of the phase function $Z(\mathbf{x})$, which are readily accessible from binary BSEM images and correspond to the porosity and two point correlation function:

$$\phi = \langle Z(\mathbf{x}) \rangle, \quad (4)$$

$$S_2(\mathrm{r}) = \langle Z(\mathrm{x}) Z(\mathrm{x}+\mathrm{r}) \rangle, \quad (5)$$

where **r** is a lag vector and angular brackets denote statistical averages. For isotropic media the two-point correlation function $S_2(\mathrm{r})$ depends only on the modulus of the lag vector, i.e. $S_2(\mathbf{r}) = S_2(r)$. Determination of $S_2(\mathrm{r})$ from binary micrographs of the pore space is typically limited to length scales of the order of 1 μm.

In small-angle scattering experiments the measured scattering intensity *I(Q)* is the Fourier transform of the density-density correlation function $\gamma(r)$:

$$I(Q) = 4\pi \int_0^\infty r^2 \gamma(r) \frac{\sin(Qr)}{Qr} dr \,, \tag{6}$$

where $\gamma(r) = (\Delta\rho)^2 \phi(1-\phi) R_Z(r)$ and $R_Z(r) \equiv (S_2(r) - \phi^2)/(\phi - \phi^2)$ is the void-void autocorrelation function and $\Delta\rho$ is a constant dependent on chemical composition and bulk density. Thus, the function $I(Q)$ measured by SANS and the function $S_2(r)$ calculated from BSEM images are a Fourier transform pair and, if $S_2(r)$ is experimentally available from BSEM images over a range of *r*-values, $I(Q)$ can be calculated in the corresponding *Q*-range using Eq. (6). The $I(Q)$ data computed in this manner are limited to relatively small *Q*-values, since the resolution of BSEM data is typically of the order of 1 μm. Detection of smaller pore length scales in the absence of SANS data is possible if the pore space exhibits surface fractal properties. For surface fractal objects of dimension D_S, the scattering intensity follows the power law $I(Q) \propto Q^{D_S - 6}$ with 2 < D_S < 3. This scaling holds in the large Q-range, but breaks down for length scales of the order of tens of micrometers, *i.e.*, for length scales of the order of grain size. The range of pore length scales over which fractal scaling applies (large *Q*-range) may be accessed by MIP using

$$-dS_{Hg}/dr \propto r^{2-D_S} \,, \tag{7}$$

where $S_{Hg}(r)$ is the sample saturation to mercury at capillary pressure $P_C \propto 1/r$. Eq. (7) is consistent with a scaling of the number-based pore size distribution according to the power law $f(r) \propto r^{-(D_S+1)}$. Over a limited range of pore length scales, $I(Q)$ data computed from $S_2(r)$ via Eq. (6) also follow the scaling $I(Q) \propto Q^{D_S-6}$, thus providing an estimate of D_S that can be compared to the one obtained by analysis of MIP data using Eq. (7). Provided that correspondence between the two values is established, one may extrapolate $I(Q)$ in the large *Q*-range according to $I(Q) \propto Q^{D_S-6}$. Thus, structural information about pore length scales not probed by BSEM may be accounted for quantitatively and consistently.

To obtain the complete distribution of pore length scales from the extended $I(Q)$ data, it is assumed that the solid-void interface has a locally spherical geometry. According to this assumption the scattering intensity per unit volume is given by:

$$I(Q) = (\Delta\rho)^2 \frac{\phi}{\langle V_r \rangle} \int_{R_{\min}}^{R_{\max}} V_r^2 f(r) F_s(Qr) dr \tag{8}$$

In Eq. (8), $R_{\max}$ and $R_{\min}$ are the maximum and minimum pore radii, respectively,

$V_r \equiv V(r) = (4/3)\pi r^3$ is the volume of a sphere of radius *r*, $\langle V_r \rangle = \int_{R_{\min}}^{R_{\max}} V_r f(r) dr$ is the average pore volume, $f(r)$ is the probability density of the pore size distribution, and $F_s(Qr)$ is the form factor for a sphere of radius r:

$$F_s(Qr) = \left[3 \frac{\sin(Qr) - Qr\cos(Qr)}{(Qr)^3} \right]^2 \tag{9}$$

The function $f(r)$ is determined by inversion of the extended $I(Q)$ data using Eq. (8). The cumulative distribution of pore volume by *pore size* is then computed from $f(r)$ and plotted along mercury porosimetry data as a function of equivalent capillary pressure for purposes of comparison.

In this paper pore size distributions obtained by DDIF-NMR and SIA are compared for three real and three synthetic porous media containing variable amounts of vuggy porosity. Furthermore, 3D magnetic resonance imaging (3D-MRI) using the basic single point imaging (SPI) pulse sequence [10] is employed as a direct, independent method for determining vug porosity and connectivity. Results of X-ray microtomography for some of the samples are reported in a companion paper.

EXPERIMENTAL METHODS

Samples: Three synthetic vuggy core plugs (3.8-cm in diameter and about 5-cm long) were made using a previously described procedure [7]. These media exhibit different amounts of vuggy porosity, generated by the dissolution of calcium carbonate particles of known size d_{CaCO_3} (see Table 1). Matrix porosity corresponds to the space between sintered glass beads of uniform size. Matrix pores vary in size depending on the choice of glass bead size (d_{GB}) and the extent of consolidation. No calcium carbonate particles were used in the making of one of these samples (SC6a), resulting in a core plug containing matrix porosity only. The real vuggy carbonate core samples (13P20H, 16BP17H and 16BP8H) are Middle Silurian dolomites from Southwestern Ontario, Canada (see Table I). Typical images of the pore space of each sample are shown in Figure 1. These images are small parts of high-resolution (1.87 μm/pixel) images of *entire* thin sections (2.6-cm wide) through each sample. Regarding the synthetic media, Figure 1 shows matrix porosity inhomogeneity in the most consolidated sample (SC16a) and the presence of *matrix* pores of size greater than the size of individual glass beads (SC6a and SC4b), corresponding to packing “flaws”. The pore space of real vuggy carbonate samples has a *self-similar* appearance. Both touching and isolated vugs are apparent in the real and synthetic media.

Sample	d_{GB} (μm)	d_{CaCO_3} (mm)	ϕ_{total} (%)	ϕ_{vug} (%)	k (mD)	F	l_c (μm)	D_s
SC16a	63-75	0.84-1.18	31.9	25.2	2406	21.2	209	-
SC6a	125-150	-	16.2	0	1040	22.1	57	-
SC4b	125-150	1.18-2.38	46.8	12.4	4740	3.1	107	-
13P20H	-	-	15.5	-	115	34.2	81	2.79
16BP17H	-	-	14.4	-	72	51.3	164	2.32
16BP8H	-	-	14.3	-	40	48.8	35	2.33

Table 1: Petrophysical properties of real and synthetic vuggy samples (whole core values). Total and vug porosities determined gravimetrically and formation factor using a 4-electrode setup. Characteristic pore diameter $\ell_c = 4\sigma\cos\theta / P_c^o$ *calculated from breakthrough capillary pressure measured using low-rate gas injection.*

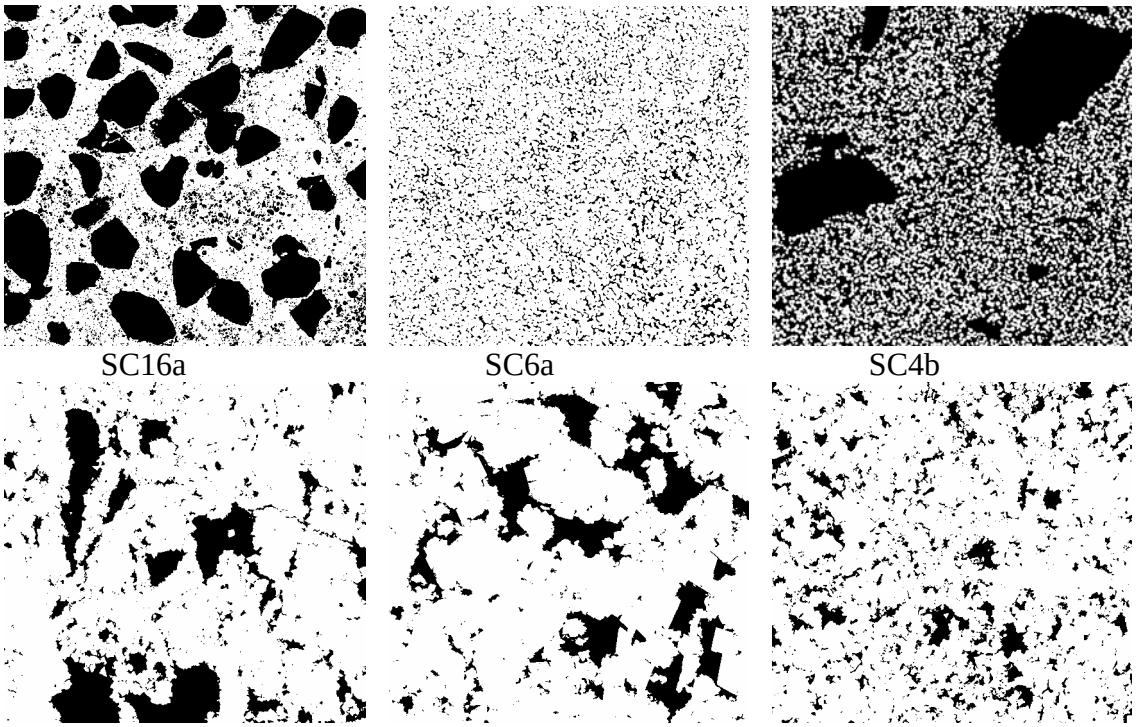

Figure 1: Representative images (cropped from images of entire thin sections) of the pore space in real and synthetic vuggy porous media. Each image represents an area of 9.2 mm x *9.8 mm.*

DDIF-NMR and 3-D MRI measurements: All NMR/MRI experiments were performed on cylindrical samples of size 0.8 cm x 0.8 cm using a Bruker 500 MHz system and a 1-cm diameter coil tuned at 500 MHz. The samples were snugly fitted into a Teflon cup and fully saturated under vacuum and pressure using de-ionized water. Away from the coil zone, a tiny cup with a drop of water was placed inside the Teflon cup to maintain 100% relative humidity and then the Teflon cup was sealed at the top.

DDIF measurements were performed using the 90° phase of the second pulse since it is less susceptible to T1 or ground state mode. For all samples, an encoding time t_e = 70 μs was used with 50 logarithmically spaced diffusion times (t_d) ranging from 10 μs to 15 s. An echo signal for every value of t_d was taken to obtain the DDIF decay curve. Each 90°-pulse was 10-μs long. The repetition rate of the pulse sequence was 4 s with 16 accumulations at each t_d to improve the signal-to-noise ratio. For MRI experiments, a reference water sample was placed right on top of the sample. MRI porosity imaging was done using the SPI pulse sequence. Three low resolution (360-μm^3 isotropic voxel) images were acquired with 30, 50 and 80-μs encoding times at 10-ms pulsing rate and another image with 30-μs encoding time at 30 ms pulsing rate to perform correction for T2 and T1 effects. One high resolution (180x180x360 μm^3/voxel) image was acquired with 50-μs encoding time at 10-ms pulsing rate and interpolated to 180-μm^3 isotropic voxel size. The reference water sample was used to determine RF inhomogeneity and to do necessary corrections. The reference sample intensity was also used for total porosity calculation. The low resolution images were extrapolated to 180μm^3/voxel after applying corrections for T2, T1 and RF inhomogeneity effects. The same correction factors were applied to the single high resolution image. The corrected low resolution images were used to determine total porosity, whereas the corrected high-resolution image was used to determine vug porosity and vug size distribution.

Figure 2a shows reference and DDIF signals for Berea sandstone. Pore size distributions determined by multi-exponential fitting [9] with are without ground state subtraction are essentially identical (Figure 2b). The pore size distribution reported here for Berea sandstone is in excellent agreement with previously published DDIF-NMR results [4].

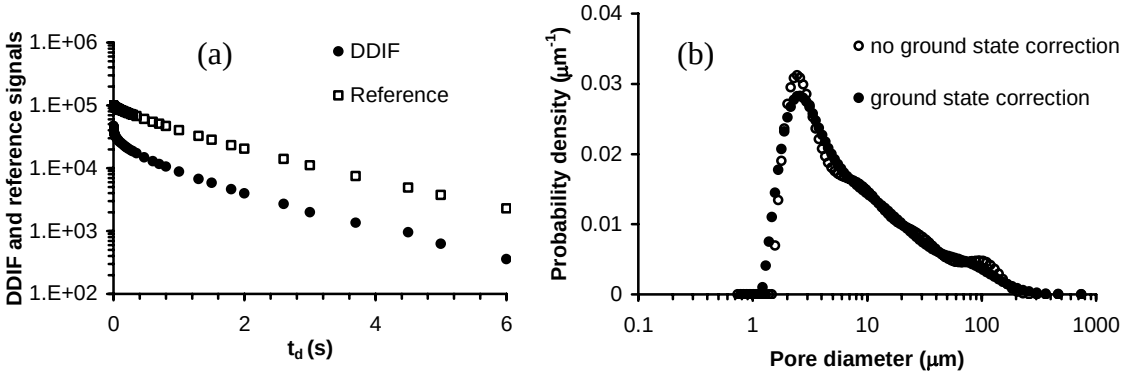

Figure 2: Cross validation of DDIF-NMR method on Berea sandstone.

MIP and statistical image analysis (SIA): The autocorrelation function $R_Z(r)$ (Figure 3a) was determined on high-resolution (1.87 μm/pixel) images of entire thin sections through the samples (Figure 1). Mercury porosimetry tests were performed on cylindrical samples 1-cm in diameter and 2-cm long. MIP data were analysed according

to Equation (7) to determine D_s (Table 1). $I(Q)$ was computed by Equation (6) using the measured $R_Z(r)$ and, for the case of real vuggy carbonate samples only, extrapolated in the large Q-range according to $I(Q) \propto Q^{D_s-6}$ using the measured D_s. The pore size distribution was determined by fitting Equation (8) to the $I(Q)$ data [8] in all cases.

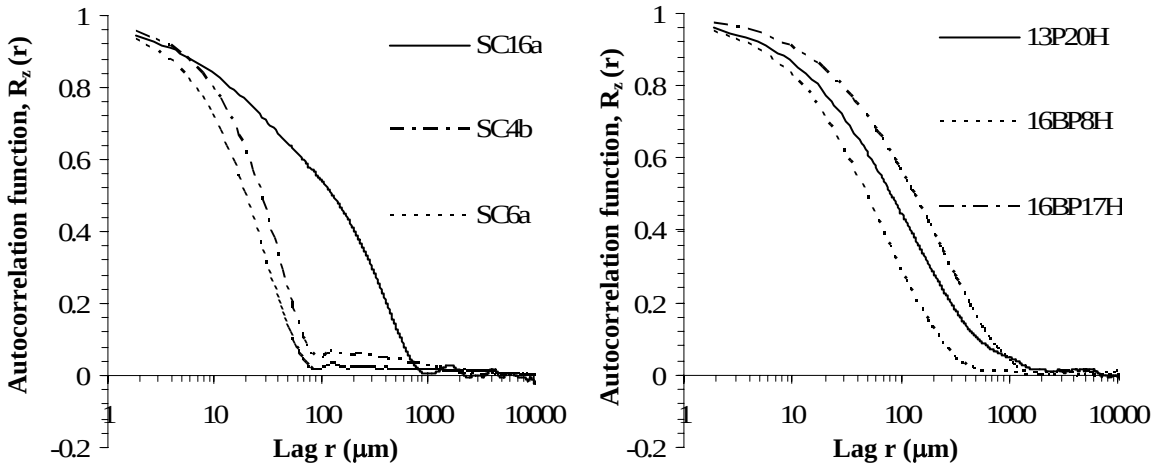

Figure 3a: Autocorrelation function measured on 2D binary images of entire thin sections.

The cumulative pore size distributions determined by DDIF-NMR and SIA also agree remarkably well (Figure 3b), considering that DDIF-NMR does not "see" pores smaller than 1 μm.

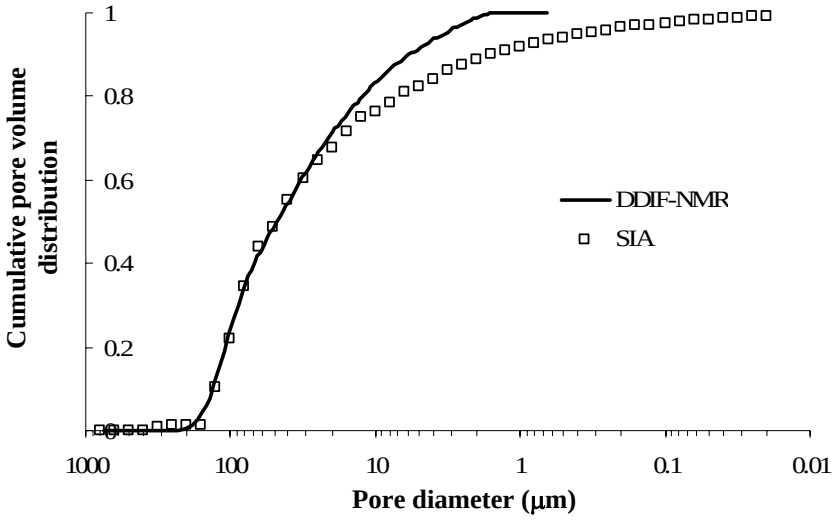

Figure 3b: Cross validation of DDIF-NMR and SIA methods on Berea sandstone.

RESULTS AND DISCUSSION

Comparison of SIA to MIP data: Pore size distributions determined by the SIA method for four of the samples are compared to mercury porosimetry data (intrusion and retraction) in Figure 4. The capillary pressure curve from SIA data is constructed from the cumulative pore volume distribution by pore size. The pore radius *r* is converted to capillary pressure using the Young-Laplace equation $P_c = 2\sigma cos\theta / r$, where σ is the surface tension of mercury (485 mN/m) and θ is the receding contact angle (40°). Capillary pressures for mercury retraction reflect the sizes of *pore bodies* from which mercury is able to retract. Using an instrument (Quantachrome Poremaster) capable of performing low-pressure mercury retraction experiments, we are able to establish consistency of the SIA data with information from mercury porosimetry. Note that SIA-based pore size distributions for all vuggy samples reflect the presence of pores in the mm-size range (vugs) – information that is not available from MIP.

Comparison of DDIF to SIA data: Figure 5 contrasts pore size distributions obtained by inversion of the DDIF-NMR decay data (without subtraction of the ground-state contribution) to those obtained by SIA. Reasonable agreement is observed, but also some notable differences. In the simplest microstructure (sample SC6a), which corresponds to narrowly distributed matrix pore sizes and no vugs, the median pore size is about 35 μm from DDIF and about 65 μm from SIA. The SIA-derived pore size distribution is skewed towards larger pore sizes, but otherwise the agreement is quite good. The next sample in order of increasing complexity is SC4b, which contains narrowly distributed matrix pores and vugs of nominal size in the range 1.2 to 2.4 mm. Again, the agreement between SIA- and DDIF-derived pore size distributions is good, but the strong bimodal character of the sample is not as evident in the DDIF results. In sample SC16a, which contains percolating vugs (average diameter of 1 mm), the SIA results reveal a mode in the 0.5-1 mm range. The mode corresponding to large pores (vugs) from DDIF is in the range 0.2-0.6 mm. Sample SC16a and all real vuggy carbonate samples are quite heterogeneous and the fact that DDIF-NMR and SIA results are based on different sample volumes (plugs 0.8-cm in diameter and 0.8-cm long for DDIF, thin-section images 2.6-cm wide for SIA) may be a factor related to the observed differences (as are several assumptions behind the interpretation of DDIF and image data). Further comparisons based on the same sample volume are discussed next.

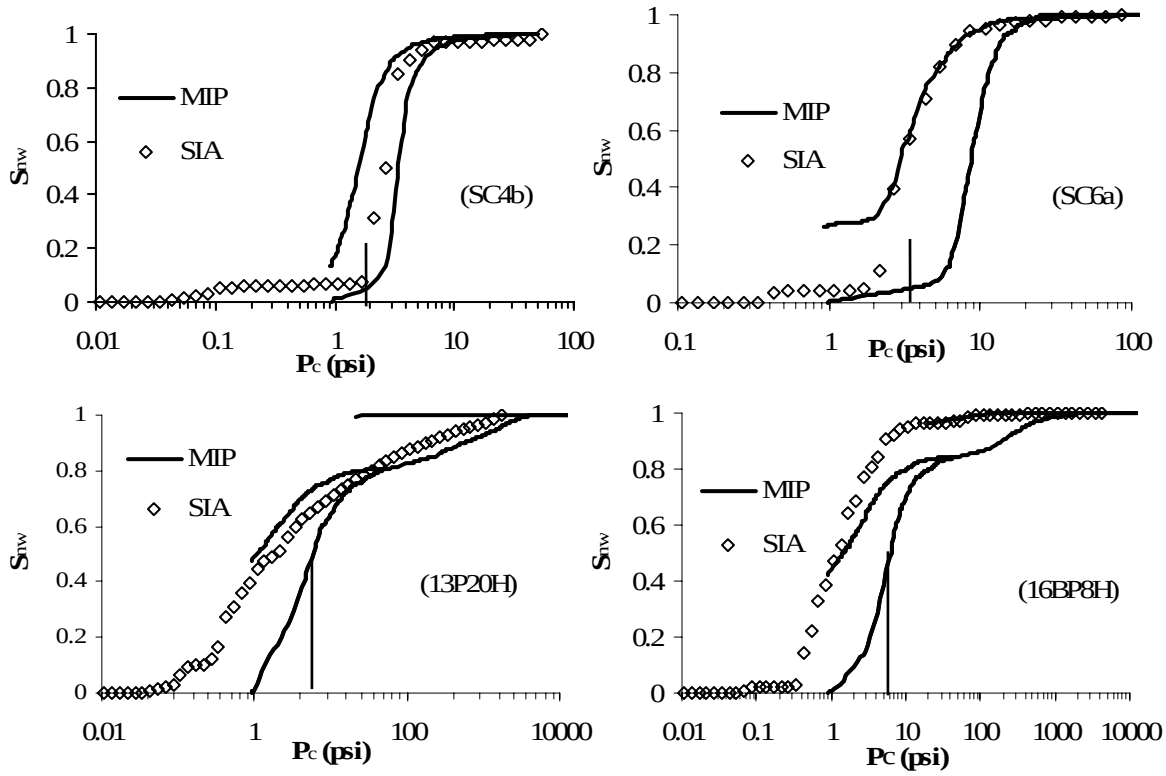

Figure 4: Representative comparisons of SIA and MIP data. Vertical lines indicate the equivalent mercury-air breakthrough capillary pressure from whole-core measurements (see Table 1).

3D MRI data: Sagital views through 3D-MRI images at 180 μm^3/voxel resolution are shown in Figure 6 for all samples. These images clearly reveal vug porosity that percolates in samples SC16a and 13P20H (Figure 6). Total porosity by MRI is compared to the saturation porosity of the same samples in Table 2. Further analysis is possible by thresholding these images to separate vug from matrix porosity and determine their relative contributions to the total porosity. A standard algorithm available in MatLab was used for this purpose. For samples SC6a, 13P20H, 16BP17H and 16BP8H vug porosity was identified with clusters comprising more than 2 voxels, more than 4 voxels for sample SC16a and more than 5 voxels from SC4b. In Table 2, the fraction of total porosity due to vugs is also compared to estimates from the DDIF-derived pore size distributions using a cut-off vug diameter of 0.2 mm (see Figure 7). From the thresholded MRI images, it is also possible to estimate the fraction of vug porosity that percolates (see Table 2). This calculation is based on determining the size of the largest percolating cluster comprising voxels identified with vugs - the results agree with visual examination of the 3D images (Figure 6).

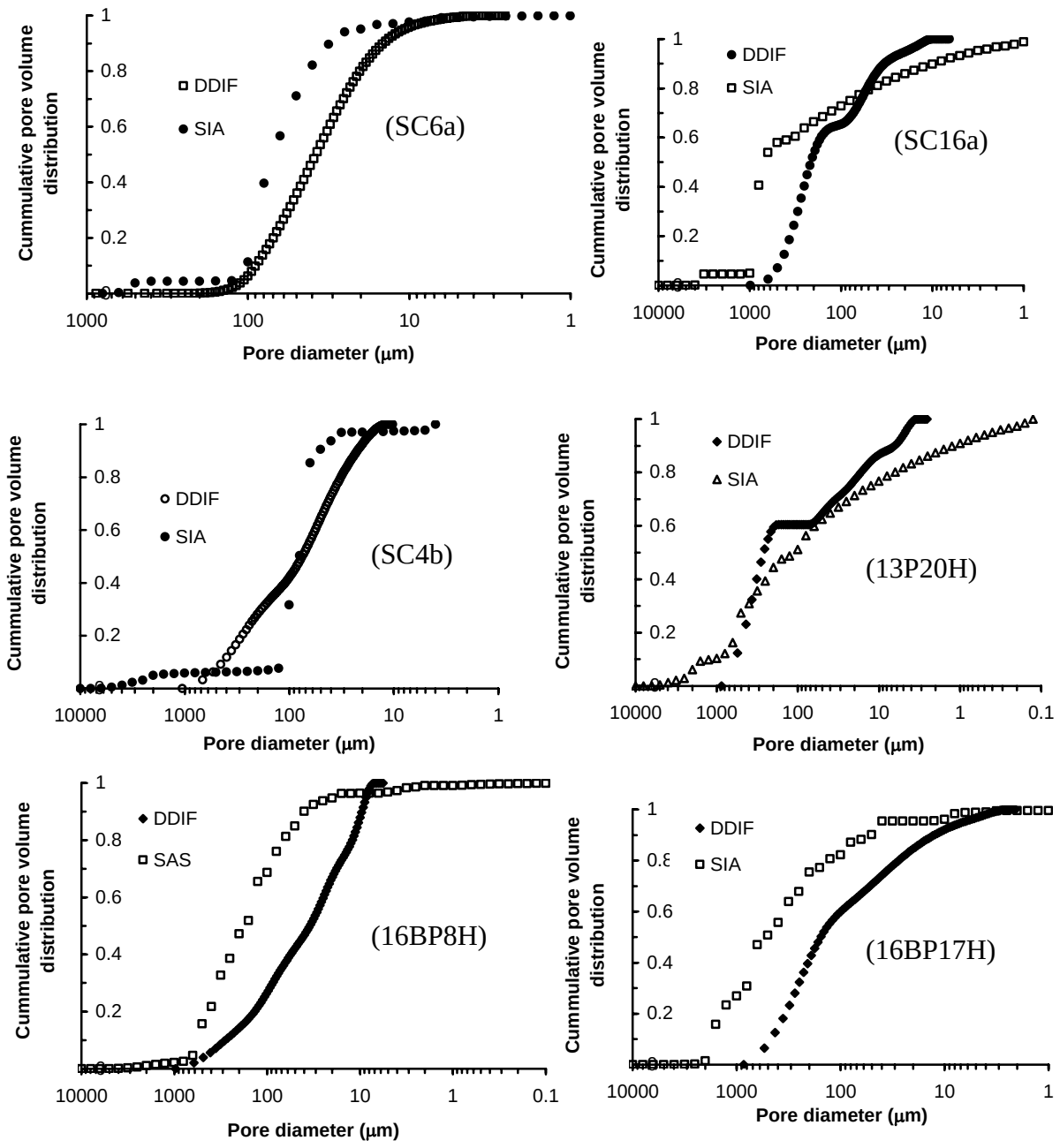

Figure 5: Pore size distribution comparisons: SIA vs. DDIF-NMR.

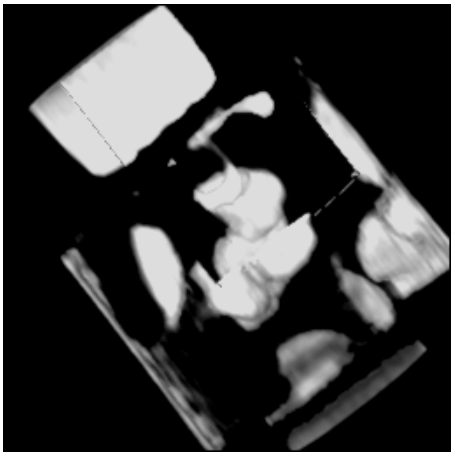

(SC4b)

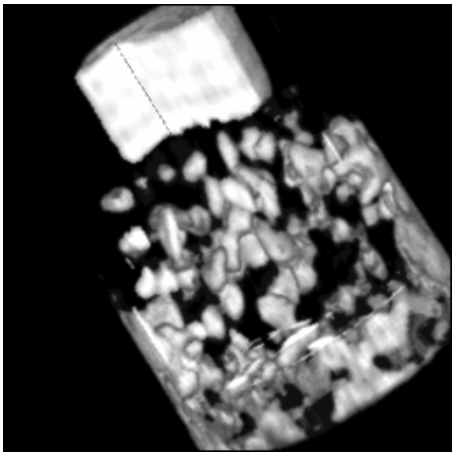

(SC16a)

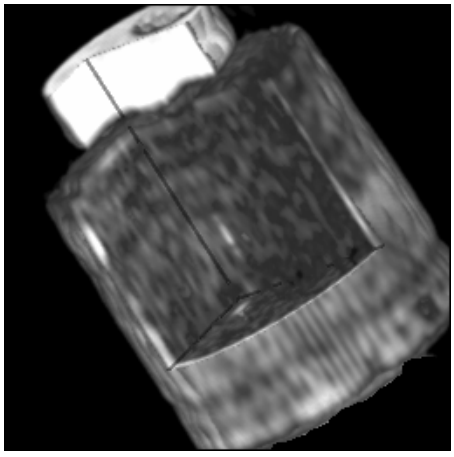

(SC6a)

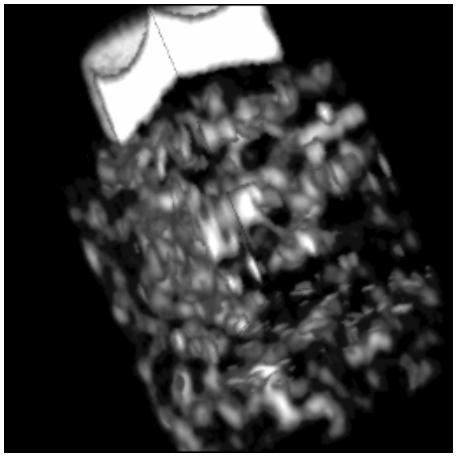

(13P20H)

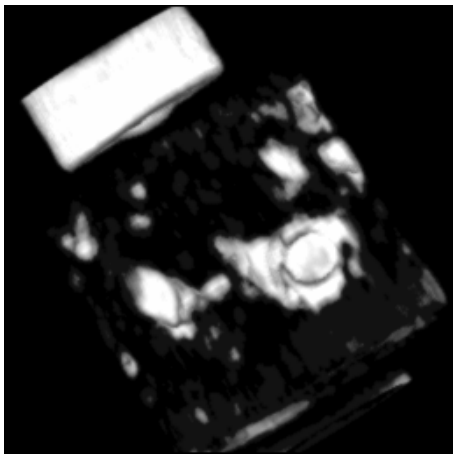

(16BP17H)

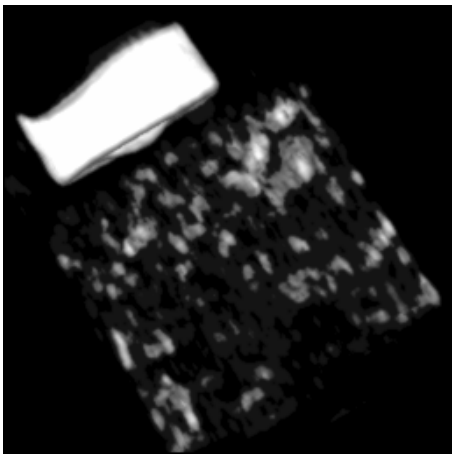

(16BP8H)

Figure 6: MRI images of porosity in real and synthetic vuggy carbonates. Reference water sample is also shown.

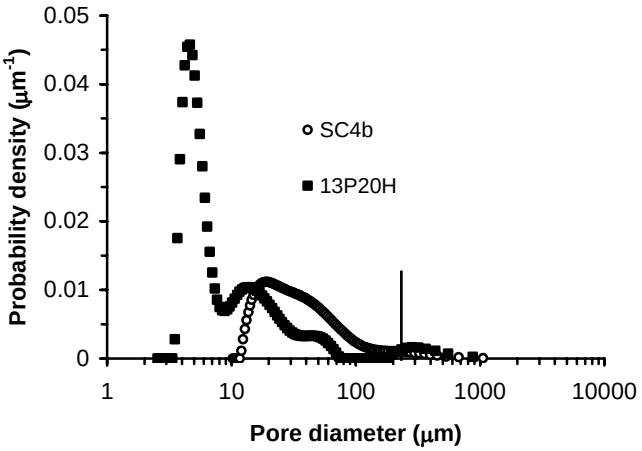

Figure 7: DDIF-NMR pore size distributions for one synthetic and one real vuggy core sample.

Sample	ϕ_{total}^{sat} (%)	ϕ_{total}^{MRI} (%)	ϕ_{vug}^{MRI} (%)	$\left(\frac{\phi_{vug}}{\phi_{total}}\right)^{MRI}$	$\left(\frac{\phi_{vug}}{\phi_{total}}\right)^{DDIF}$	f_p
SC16a	30.1	28.2	18.4	0.65	0.65	0.945
SC6a	19.7	21.4	0	0	0	0
SC4b	43.9	35.1	10.1	0.29	0.35	0
13P20H	19.8	19.4	11.5	0.59	0.61	0.819
16BP17H	15.3	13.9	8.4	0.60	0.60	0
16BP8H	18.6	17.4	11.2	0.64	0.28	0

Table 2: Results of porosity measurements (by saturation, MRI and DDIF-NMR methods) on small cylindrical plugs of size 0.8 cm x 0.8 cm. f_p *is the fraction of vug porosity that percolates.*

CONCLUSIONS

- DDIF-NMR, 3D MRI, statistical image analysis (SIA) and mercury porosimetry methods were successfully integrated to investigate matrix and vug porosity in real and model vuggy carbonates.
- Model vuggy samples synthesized by sintering/dissolution of glass beads and calcium carbonate particles exhibit well-controlled microstructures that, albeit simpler, are useful analogues of real vuggy carbonates.
- The microstructure data obtained in this work constitute a self-consistent background on which interpretation of petrophysical measurements may be based and network modeling predictions tested.
- The potential of combined DDIF-NMR/MRI methods to reveal the amount, size distribution and degree of connectivity was demonstrated.

MRI is limited in resolution – higher resolution 3D images can be obtained by x-ray microtomography – whereas DDIF-NMR derived pore size distributions show remarkable agreement with those obtained by the SIA method. The differences between the two may be traced in part to sample inhomogeneity and in part to the simplifying assumptions behind the SIA and DDIF methods. The level of agreement observed indicates that a deeper theoretical investigation of DDIF-NMR in multiscale porous media is warranted to test the validity of the assumptions made to determine the pore size distribution (a work that is under progress).

REFERENCES

1. Ioannidis, M.A. and Chatzis, I. (2000): "A Dual-Network Model of Pore Structure for Vuggy Carbonates", *Proceedings of the Annual Symposium of the Society of Core Analysts*, SCA2000-09, Abu Dhabi, U.A.E.
2. Moctezuma, A., Bekri, S., Laroche, C. and Vizika, O. (2003): "A Dual-Network Model for Relative Permeability of Bimodal Rocks: Application in a Vuggy Carbonate", *Proceedings of the Annual Symposium of the Society of Core Analysts*, SCA2003-94, Pau, France.
3. Song, Y., Ryu, S. and Sen, P. (2000): "Determining Multiple Length Scales in Rocks", *Nature*, **406**, 178.
4. Chen, Q., Butler, K.E., Gingras, M.K. and Balcom, B.J. (2005): "A Mechanism Study of Co-Current and Counter-Current Imbibition Using New Magnetic Resonance Techniques", *Proceedings of the Annual Symposium of the Society of Core Analysts*, SCA2005-38, Toronto, Canada.
5. Radlinski, A.P., Ioannidis, M.A., Hinde, A.L., Hainbuchner, M., Baron, M., Rauch, H, and Kline, S. (2004): "Angstrom-to-Millimeter Characterization of Sedimentary Rock Microstructure", *J. Colloid Interface Sci.*, **274**, 607.
6. Amirtharaj, E.S., Ioannidis, M.A. and Macdonald, I.F. (2003): "Statistical Synthesis of Image Analysis and Mercury Porosimetry for Multiscale Pore Structure Characterization", *Proceedings of the Annual Symposium of the Society of Core Analysts*, SCA2003-10, Pau, France.
7. Padhy, G., M. A. Ioannidis and C. Lemaire (2005): "Special Core analysis studies in Vuggy porous media of controlled microstructure", *Proceedings of the Annual Symposium of the Society of Core Analysts*, SCA2005-76, Toronto, Canada.
8. Hinde, A.L. (2004): "PRINSAS: A Windows-based Computer Program for the Processing and Interpretation of Small-Angle Scattering Data Tailored to the Analysis of Sedimentary Rocks", *J. Appl. Crystallography*, **37**, 1020.
9. Venkataramanan, L., Song, Y. and Hurlimann, M.D. (2002): "Solving Fredholm Integrals of the First Kind with Tensor Product Structure in 2 and 2.5 Dimensions", *IEEE Trans. Signal Processing*, **50**, 1017.
10. Emid, S. and Creyghton, J.H.N. (1985): "High Resolution NMR Imaging in Solids " , Physica **128B**, 81-83.